Journal of Alloys and Compounds 512 (2012) 230–234

Contents lists available at SciVerse ScienceDirect

Journal of Alloys and Compounds

journal homepage: www.elsevier.com/locate/jallcom

Effective segregation during Czochralski growth and spectral properties of Nd^{3+} in GSAG crystal

J. Su[a,*], B. Liu[a], L.H. Xu[a], Q.L. Zhang[b], S.T. Yin[b]

[a] College of Math and Physics, Nanjing University of Information Science and Technology, Nanjing 210044, China
[b] Anhui Institute of Optics and Fine Mechanics, Chinese Academy of Sciences, Hefei 230031, China

ARTICLE INFO

Article history:
Received 29 May 2011
Received in revised form
20 September 2011
Accepted 22 September 2011
Available online 29 September 2011

Keywords:
Crystal growth
Optical materials
Optical spectroscopy
Luminescence

ABSTRACT

GSAG and Nd:GSAG crystals were grown by standard Czochralski technique. The refractive index of GSAG in the wavelength range 500–3000 nm, effective segregation coefficient and absorption cross sections of Nd^{3+} in GSAG were determined by optical absorption method. The effective segregation coefficient was calculated to be 0.525. The spectroscopic and laser properties of Nd:GSAG crystal were studied by Judd–Ofelt analysis. The Judd–Ofelt parameters were calculated to be $\Omega_2 = 1.32 \times 10^{-21}$ cm^2, $\Omega_4 = 2.93 \times 10^{-20}$ cm^2 and $\Omega_6 = 3.91 \times 10^{-20}$ cm^2. With these intensity parameters, the values of absorption and emission oscillator strengths, transition probabilities, fluorescence ratios and radiative lifetimes were obtained. The large fluorescence ratio of $|[4F]3/2\rangle$ is very favorable for laser operation at 942 nm. These results confirm that Nd:GSAG is a suitable laser material for water vapor detection by DIAL.

1. Introduction

Up to now, the measurement of water vapor in atmosphere with sufficient vertical resolution and global accuracy is still a challenge work. To solve this problem, a differential absorption lidar (DIAL) in the wavelength regions of 935 nm, 942 nm or 944 nm is needed [1]. Although these laser wavelengths can be obtained by optical parametric oscillator (OPO), Ti:Sapphire laser and Raman-shifter, such systems are complicated and expensive, which limited their space applications. At present, garnet crystals like Nd:GSAG, Nd:GSGG, Nd:YGG, etc. are of high interest because the above wavelengths can be obtained by pumping these garnet crystals with laser diode (LD). Among these garnet crystals, Nd:GSAG crystal has attracted more attentions. Kallmeyer et al. reported its growth, emission cross-section and demonstrated its application for water vapor detection [2]. Wang et al. gave the model of pulsed Nd:GSAG laser at 942 nm [3]. Eichler et al. compared the different laser systems with efficient 935/942 nm laser, including stimulated Raman scattering lasers, Ti:Sapphire lasers and Diode-pumped lasers of Nd:GSAG and Nd:YGG, they have pointed out that the compact, high-efficient, diode-pumped solid state laser with long life is very promising for space application [4]. Strohmaier et al. [5] and Zhang et al. [6] also reported the diode-pumped Nd:GSAG and Nd:YGG lasers at 942 nm and 935 nm. Recently, stable LD-pumped mode-locked and tunable single frequency injection-seeded Q-switched Nd:GSAG lasers around 942 have been demonstrated for the further development of quasi-three-level Nd^{3+} lasers [7,8].

It is well known that dopant segregation is an important characteristic in Czochralski growth. However, the reports on the effective segregation coefficient k of Nd^{3+} in GSAG during crystal growth were seldom. We determined the refractive index of GSAG in a wider wavelength range, and then the k value was concisely obtained by optical absorption method, which is the first report to our knowledge.

Judd–Ofelt parameter calculation [9,10] is a popular method used to analyze spectroscopic properties of rare earth ions. Sumida et al. reported the laser-related properties of Cr:Nd:GSAG crystal, and used this theory to analysis of the spectrum of Nd^{3+} in GSAG crystal by subtracting the contribution of Cr^{3+} ions to the codoped spectrum [11]. In our work, Judd–Ofelt theory was used to analysis the spectroscopic and lasing properties of Nd:GSAG, our results should be more concise and complete because all the analyses were based on the effective segregation coefficient from our experiments and the measured aborsorption spectra of Nd:GSAG.

2. Experimental

2.1. Crystal growth

GSAG and Nd:GSAG crystals were grown by the standard Czochralki technique with a medium frequency heated and iridium crucible. Oxides with purity 99.999% were used as starting materials. Gd_2O_3, Sc_2O_3 and Al_2O_3, total 1800 g in weight were mixed in a molar ratio Gd:Sc:Al = 3:2:3. The oxide mixture were pressed into pellets and sintered in air at 1200 °C for 24 h, then put into iridium crucible, and the

* Corresponding author. Tel.: +86 25 58731031; fax: +86 25 58731174.
E-mail address: zlj007@126.com (J. Su).

0925-8388/$ – see front matter © 2011 Elsevier B.V. All rights reserved.
doi:10.1016/j.jallcom.2011.09.071

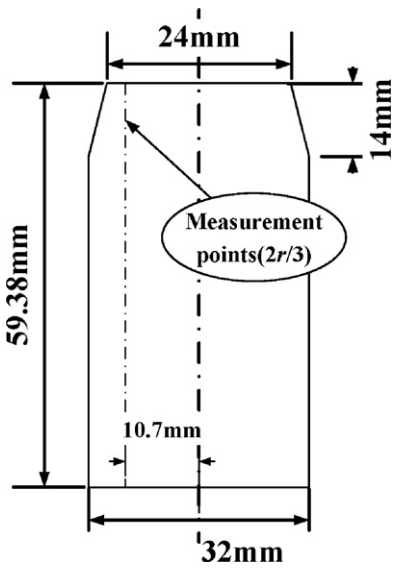

Fig. 1. Schematic diagram of Nd:GSAG slab used to measure absorption spectra.

temperature was raised until the charge had completely melt. Nd:GSAG crystal was grown by adding 15 g Nd_2O_3 to the above 1800 g oxide mixture. With GSAG seed crystals, GSAG and Nd:GSAG crystals were grown along ⟨1 1 1⟩ direction.

2.2. Absorption measurement

A GSAG disk was cut perpendicular to ⟨1 1 1⟩ growth direction and optically polished with thickness of 2 mm. The transmission spectrum in the range 500–3000 nm was recorded using a Lambda 900 (Perkin Elmer) spectrometer.

A slab was cut from the grown Nd:GSAG crystal, at the core along ⟨1 1 1⟩ direction, it was optically polished with thickness of 2.9 mm. The sizes of the slab section were shown in Fig. 1. A series of transmission spectra were measured with Lambda 900 spectrometer, the incident light was perpendicular to the slab section at the points of $2r/3$ (r is maximum radius) from the core with longitudinal interval of 5 mm, as Fig. 1 shows. All the measurements were completed at room temperature.

3. Results and discussion

3.1. Refractive index determined by optical absorption

The refractive index behaviors of garnets in the range of 535–645 nm have been reported by Wemple and Tabor [12]. In order to obtain the refractive index of GSAG in a wider wavelength range, we measured the absorption spectrum of GSAG in the range of 500–3000 nm, in which it is transparent optically. The refractive index n of GSAG crystal can be calculated according to the formula [13]:

$$R = \frac{1-T}{1+T} \tag{1}$$

$$n = \frac{1+\sqrt{R}}{1-\sqrt{R}} \tag{2}$$

where T is the transmissivity, R is reflectivity on the crystal surface, then we got the values of the refractive index square n^2, and the experimental curve of $n^2 \sim \lambda$ was shown in Fig. 2. These experimental data were fitted using a least-square fitting program to the following Sellmeier equation:

$$n^2 = A + \frac{B}{\lambda^2 - C} - D\lambda^2 \tag{3}$$

The values of A, B, C and D are fitted as 3.71473, 7.07794 nm^2, 2197169.40578 nm^2, 2.9697×10^{-8} nm^{-2}, respectively. Fig. 2 shows that the experimental and fitting values agree well. In the following analysis, Eq. (3) was used to recalculate the values of

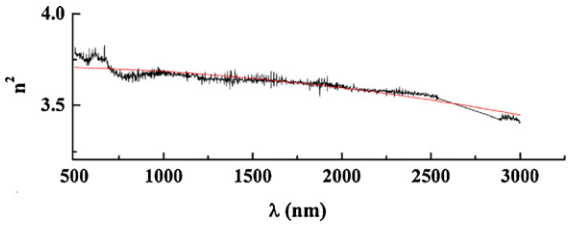

Fig. 2. Fitting curve of refractive index of GSAG crystal.

appropriate indices of refractive at the appropriate mean wavelengths of absorption by the Nd^{3+} ion.

3.2. Effective segregation coefficient and absorption cross-section of Nd^{3+} in GSAG

According to the analysis in Ref. [14], as the segregated dopant disperses into melt homogenously, the solute concentration in the crystal C_S at growth interface would change with the grown crystal mass W_S by

$$C_S = kC_0\left(1 - \frac{W_S}{W_T}\right)^{k-1} \tag{4}$$

where W_T is the total mass of raw material used to grow crystal, C_0 is the initial solute concentration, and k is effective segregation coefficient. In the case that segregated dopant disperses into melt partly, C_S would changes by

$$C_S = kC_0 e^{(k-1)(W_S/\Delta W)} \tag{5}$$

where ΔW is the mass of the grown melt into which dopant disperses.

For optical absorption ions, the C_S can be related to their absorption coefficient α by

$$\alpha = \frac{AN_A\sigma\rho}{M_d}C_S \tag{6}$$

where A and M_d are dopant ion number per molecular and molecular weight of doped compound, respectively, σ is absorption cross section in 10^{-20} cm^2, ρ is the host density and N_A is Avogadro constant. Ref. [14] gives a formula to calculate the absorption coefficients α in cm^{-1} of crystal with T, but there is a minor error in it, the formula should be corrected as

$$\alpha_{ij}^{exp} = -\frac{1}{d}\ln\frac{-(1-R_i)^2 + \sqrt{(1-R_i)^4 + 4R_i^2T_{ij}^2}}{2R_i^2T_{ij}} \tag{7}$$

where i and j stand for the ith absorption peak and jth measure point on crystal, respectively, d is the sample thickness, $R_i = ((n_i-1)/(n_i+1))^2$. With different grown crystal mass, the absorption coefficients at different wavelengths are shown in Table 1.

Fitting relative residual is defined as

$$R_S = \sqrt{\frac{\sum_{i,j}(\alpha_{ij}^{exp} - \alpha_{ij})^2}{\sum_{ij}(\alpha_{ij}^{exp})^2}} \tag{8}$$

with the calculation method reported in Ref. [14], the values of k and σ or k and ΔW were obtained. The values of absorption cross section σ are shown as in Table 2, the value of k fitted is 0.525, and the fitting relative residual R_S is 0.62%. With the obtained values of σ, the fitted values of k, ΔW, R_S are 0.525, 1655.9 g, 0.63%, respectively. All of the fitted results are consistent with experimental values.

The effective segregation coefficient k of Nd^{3+} in GSAG (0.525) is much higher than that in YAG (0.1–0.2), which would be very favorable for grow high-doped crystals with high-optical quality.

Table 1
Absorption coefficients α with different grown crystal mass W_S and at different wavelengths λ.

λ (nm)\α (cm^{-1})\W_S (g)	264.47	241.83	219.20	196.56	173.93	151.29	128.66	106.02	83.39	66.48	46.99	30.76
821.4	0.722	0.7123	0.7063	0.7099	0.6569	0.6694	0.6997	0.6938	0.6955	0.688	0.6894	0.697
816.6	1.9975	1.973	1.9646	1.9624	1.9028	1.9019	1.9233	1.9081	1.8913	1.879	1.8831	1.883
809	5.3212	5.2852	5.2282	5.2426	5.164	5.1234	5.1043	5.0715	5.0312	5.0088	4.9821	4.96
805.1	2.2106	2.187	2.1685	2.1765	2.1091	2.0991	2.112	2.1034	2.0937	2.0755	2.0733	2.066
798.3	1.2346	1.2183	1.198	1.2019	1.1508	1.1487	1.1781	1.1725	1.1652	1.1519	1.1515	1.15
795.6	2.8724	2.8581	2.8248	2.8387	2.7667	2.7607	2.7626	2.7566	2.7229	2.7051	2.6982	2.6
792.1	1.2336	1.2354	1.2054	1.2121	1.1614	1.1633	1.1861	1.1815	1.1748	1.1612	1.1692	1.1
778.8	0.3552	0.3511	0.3445	0.3479	0.3076	0.3274	0.346	0.3461	0.3532	0.3434	0.3416	0.35
759.9	1.0815	1.072	1.0683	1.0659	1.0149	1.0202	1.0465	1.0438	1.0339	1.0317	1.0258	1.02
755.3	2.3095	2.2901	2.2765	2.2794	2.2149	2.2054	2.2162	2.2056	2.1915	2.1732	2.1787	2.1
749.2	2.7553	2.7365	2.7073	2.7128	2.6502	2.6373	2.645	2.6247	2.6066	2.586	2.5794	2.572
743.9	2.5686	2.545	2.5255	2.5227	2.4617	2.4467	2.449	2.4381	2.4198	2.4083	2.4051	2.398
737.2	3.1989	3.1828	3.1455	3.1548	3.0883	3.0679	3.0744	3.0544	3.0244	3.0028	2.9993	2.9
733.3	0.9798	0.9799	0.9689	0.9691	0.9262	0.9279	0.9525	0.9479	0.94	0.9329	0.9267	0.934

Table 2
Absorption cross sections of Nd^{3+} in GSAG crystal.

λ (nm)	σ (10^{-20} cm^2)	λ (nm)	σ (10^{-20} cm^2)	λ (nm)	σ (10^{-20} cm^2)	λ (nm)	σ (10^{-20} cm^2)
821.4	0.7111	798.3	1.2046	759.9	1.0687	737.2	3.1541
816.6	1.9674	795.6	2.8366	755.3	2.2775	733.3	0.9709
809	5.2476	792.1	1.215	749.2	2.7132		
805.1	2.1725	778.8	0.351	743.9	2.5234		

The value of ΔW 1655.9 g is very close to the mass of the raw materials used to grow crystal, which indicates that the segregated Nd^{3+} during crystal growth disperse nearly into the whole melt, and the transport status of Nd^{3+} in melt is quite well.

3.3. Judd–Ofelt analysis of the Nd^{3+} absorption intensities in Nd:GSAG

3.3.1. Judd–Ofelt theory

According to Judd–Ofelt theory [9,10], the electric dipole (ed) line strength, magnetic dipole (md) line strength of rare earth ion from $|i\rangle = |[\alpha SL]J\rangle$ to $|i'\rangle = |[\alpha' S' L']J'\rangle$ can be given by:

$$S_{ii'}^{\mathrm{ed}} = \sum_{t=2,4,6} \Omega_t (\langle [\alpha' S' L'] J' || U^t || [\alpha SL] J \rangle)^2 \tag{9}$$

$$S_{ii'}^{\mathrm{md}} = \left(\frac{h}{4\pi mc}\right)^2 \langle [\alpha' S' L'] J' || \vec{\mathbf{L}} + 2\vec{\mathbf{S}} || [\alpha SL] J \rangle^2 \tag{10}$$

where h is plank constant, m is electron mass, c is light speed. Ω_t are the Judd–Ofelt parameters, which can be derived by a least square fitting of experimental and theoretical electric oscillator strengths.

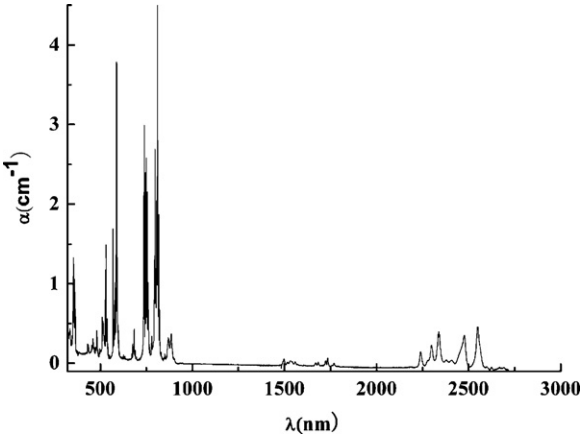

Fig. 3. Absorption spectrum of Nd:GSAG crystal.

$\langle ||U^{(t)}|| \rangle$ are the reduced matrix elements, which are not sensitive to hosts and can be found in Ref. [9].

The calculated oscillator strength $f_{ii'}$ and the total radiative transition probability $A_{ii'}$ are expressed as

$$f_{ii'} = \frac{\chi}{n^2} \frac{8\pi^2 mc}{3h(2J+1)\lambda} S_{ii'} \tag{11}$$

$$A_{ii'} = \chi \frac{16\pi^3 e^2}{3h\varepsilon_0 (2J+1)\lambda^3} S_{ii'} \tag{12}$$

where n, ε_0, e are medium refractive index, dielectric constant and electron charge, respectively. χ is medium corrective factor, which is $n^2(n^2+2)^2/9$ for electric dipole transition and n^3 for magnetic dipole transition. λ is average transition wavelength and can be calculated by

$$\lambda = \frac{\int_{\mathrm{band}} \lambda' \alpha(\lambda')\, d\lambda'}{\int_{\mathrm{band}} \alpha(\lambda')\, d\lambda'} \tag{13}$$

The fluorescence branching ratio β and the radiative lifetime τ can be obtained by

$$\beta_{ii'} = \frac{A_{ii'}}{\sum_{i'} A_{ii'}} \tag{14}$$

$$\tau_i = \frac{1}{\sum_{i'} A_{ii'}} \tag{15}$$

Experimental oscillator strength $f_{ii'}^{\mathrm{exp}}$ can be calculated by

$$f_{ii'}^{\mathrm{exp}} = f_{ii'}^{\mathrm{ed}} + f_{ii'}^{\mathrm{md}} = \frac{4\varepsilon_0 mc^2}{Ne^2 \bar{\lambda}^2} \int \alpha(\lambda)\, d\lambda \tag{16}$$

where N is the Nd^{3+} ion concentration. $f_{ii'}^{\mathrm{md}}$ can be calculated by (10) and (11) directly, then the experimental electric pole oscillator strength can be obtained by

$$f_{ii'}^{\mathrm{ed,exp}} = f_{ii'}^{\mathrm{exp}} - f_{ii'}^{\mathrm{md,cal}} \tag{17}$$

The fitting quality can be evaluated by residual error R_S, which is defined by:

$$R_S = \left(\frac{\sum_{i'} (f_{ii'}^{\mathrm{ed,exp}} - f_{ii'}^{\mathrm{ed,cal}})^2}{(f_{ii'}^{\mathrm{ed,exp}})^2} \right)^{1/2} \tag{18}$$

Table 3
Calculated and measured line strengths and oscillator strengths for the absorption transitions of Nd^{3+} in GSAG (the initial state is $^4I_{9/2}$).

Transitions	Band (nm)	λ (nm)	$f^{ed,exp}$ (10^{-6})	$f^{ed,cal}$ (10^{-6})	$S^{ed,exp}$ (10^{-20} cm^2)	$S^{ed,cal}$ (10^{-20} cm^2)	S^{md} (10^{-20} cm^2)	f^{md} (10^{-6} cm^2)
|[4*I*]13/2⟩	2207–2635	2418	1.34	1.60	1.52	1.82	0	0
|[4*I*]15/2⟩	1475–1783	1616	0.70	0.23	0.55	0.18	0	0
|[4*F*]3/2⟩	841–914	875	1.67	2.07	0.71	0.88	0	0
|[4*F*]5/2⟩	778	805	7.26	6.94	2.85	2.72	0	0
|[2*H*]9/2⟩	–830						0.03	0.09
|[4*F*]7/2⟩	723	746	7.09	7.45	2.58	2.71	4.2×10^{-6}	1.2×10^{-5}
|[4*S*]3/2⟩	–768						0	0
|[4*F*]9/2⟩	671–697	682	0.62	0.57	0.21	0.19	8.2×10^{-3}	0.03
|[4*G*]5/2⟩	5621	584	7.43	7.47	2.12	2.13	0	0
|[4*G*]7/2⟩	–607						1.3×10^{-5}	4.7×10^{-5}
|[4*G*]7/2⟩	496	522	4.94	4.47	1.2621	1.14	2.4×10^{-5}	9.5×10^{-5}
|[4*G*]9/2⟩	–541						3.5×10^{-3}	1.4×10^{-2}
|[2*K*]13/2⟩							0	0
|[4*G*]11/2⟩							4.7×10^{-4}	2.1×10^{-3}
|[2G_1]9/2⟩	450	470	2.32	1.18	0.53	0.27	7.8×10^{-4}	3.5×10^{-3}
|[2D_1]3/2⟩	–490						0	0
|[2*K*]15/2⟩							0	0
|[2*P*]1/2⟩	427–440	434	0.35	0.51	0.075	0.11	0	0
|[4*D*]3/2⟩							0	0
|[4*D*]5/2⟩							0	0
|[2*I*]11/2⟩	340	356	10.40	10.54	1.81	1.84	0	0
|[4*D*]1/2⟩	–373						1.3×10^{-3}	7.6×10^{-3}
|[2*L*]7.5⟩							0	0

3.3.2. Spectral analysis of Nd:GSAG

Using the effective segregation coefficient $k = 0.525$, density $\rho = 5.998$ g/cm^3, $C_0 = 15/1800$, $W_S/W_T = 30.76/1800$, the concentration of Nd^{3+} were calculated to be $N = 9.467\times10^{19}$ cm^{-3}. The absorption coefficient can be calculated by Eq. (7) and the absorption spectrum of Nd^{3+} in GSAG is shown in Fig. 3.

The values of experimental and calculated line strengths and oscillator strengths are shown in Table 3. It shows that the line strengths and oscillator strengths of magnetic dipole transitions are weaker by 2–3 orders of magnitude than those of electric dipole transitions. The Judd–Ofelt intensity parameters Ω_t ($t = 2, 4, 6$) are fitted to be $\Omega_2 = 1.32\times10^{-21}$ cm^2, $\Omega_4 = 2.93\times10^{-20}$ cm^2 and $\Omega_6 = 3.91\times10^{-20}$ cm^2 with $R_s = 8.7\%$. With the intensity parameters Ω_t ($t = 2, 4, 6$), the line strengths, oscillator strengths, radiative transition probabilities, fluorescence branch ratios and radiative times, etc. were calculated. The results were listed in Table 4.

During the above calculations, the absorption transition of \|[4*F*]5/2⟩ and \|[2*H*]9/2⟩ were separated using multi-peak fitting with Lorentzian peak profiles. The data in the ranges of 789–823 nm, 776–789 nm were fitted separately. Meanwhile, the baseline was subtracted before fitting in the range 789–823 nm, which improved the fitting obviously. The fitting results were shown in Fig. 4. It shows that the fitting curves are consistent with the experimental values very well. According to the energy level assignment of $Nd:Gd_3Ga_5O_{12}$ and $Nd:Lu_3Al_5O_{12}$ [15], the separated peaks were assigned as the following:

\|[4*I*]9/2⟩ → \|[4*F*]5/2⟩: 798.31, 800.25, 803.89, 805.17, 808.99, 809.75, 811.42, 816.57, 821.41 (in nm)
\|[4*I*]9/2⟩ → \|[2*H*]9/2⟩: 778.63, 781.23, 784.94, 788.83, 792.1, 795.50 (in nm)

The site symmetry of Nd^{3+} in GSAG is D_2. The multiplets $J = 9/2$ and $J = 5/2$ in D_2^* were split into $3\Gamma_5$ and $5\Gamma_5$, respectively. Although the split number of $J = 5/2$ is less than that of $J = 9/2$, the transition line strength of \|[4*I*]9/2⟩ → \|[4*F*]5/2⟩ is stronger than that of \|[4*I*]9/2⟩ → \|[2*H*]9/2⟩ by one order, as a result, some absorption peaks of \|[4*I*]9/2⟩ → \|[2*H*]9/2⟩ could not be discerned at room

Table 4
Calculated results of the optical transition parameters of Nd:GSAG crystal.

|*i*⟩, *E* (cm^{-1}), τ (μs)	|*i'*⟩	λ (nm)	S^{ed} (10^{-20} cm^2)	S^{md} (10^{-20} cm^2)	f^{ed} (10^{-6})	f^{md} (10^{-6})	A_{ed} (s^{-1})	A_{md} (s^{-1})	β (%)
|[2*H*]9/2⟩, 12,551.6, 1164	|[4*F*]5/2⟩	47,103	0.11	0	0.18	0	0.37	0	0.04
	|[4*F*]3/2⟩	8615	0.13	0	0.05	0	0.24	0	0.03
	|[4*I*]15/2⟩	1565	0.92	0	1.22	0	125.6	0	14.6
	|[4*I*]13/2⟩	1184	0.47	0	0.82	0	147.2	0	17.1
	|[4*I*]11/2⟩	963	0.10	0.01	0.21	0.03	55.94	7.7	7.4
	|[4*I*]9/2⟩	795	0.48	0.03	1.23	0.09	485.4	36.2	60.8
|[4*F*]5/2⟩, 12,366.3, 186	|[4*F*]3/2⟩	10,543	0.16	0.34	0.10	0.15	0.40	0.64	0.02
	|[4*I*]15/2⟩	1618	0.90	0	1.93	0	186.3	0	3.5
	|[4*I*]13/2⟩	1214	2.10	0	5.94	0	1008.9	0	18.7
	|[4*I*]11/2⟩	983	0.63	0	2.21	0	570.0	0	10.6
	|[4*I*]9/2⟩	809	2.25	0	9.49	0	3626.5	0	67.2
|[4*F*]3/2⟩, 11,417.8, 241	|[4*I*]15/2⟩	1913	0.11	0	0.31	0	21.5	0	0.52
	|[4*I*]13/2⟩	1373	0.81	0	3.05	0	408.8	0	9.8
	|[4*I*]11/2⟩	1084	2.02	0	9.58	0	2038.8	0	49.1
	|[4*I*]9/2⟩	876	0.88	0	5.18	0	1684.5	0	40.6
|[4*I*]15/2⟩, 6189.2, 13,200	|[4*I*]13/2⟩	4869	6.01	0.71	1.82	0.21	22.7	2.58	33.3
	|[4*I*]11/2⟩	2504	1.67	0	0.84	0	36.7	0	48.4
	|[4*I*]9/2⟩	1615	0.18	0	0.14	0	13.8	0	18.2
|[4*I*]13/2⟩, 4135.8, 13,573	|[4*I*]11/2⟩	5154	5.24	0.93	1.74	0.30	19.7	3.4	31.3
	|[4*I*]9/2⟩	2418	1.82	0	1.14	0	50.6	0	68.7
|[4*I*]11/2⟩, 2195.7, 30,517	|[4*I*]9/2⟩	4554	4.87	0.69	2.07	0.28	28.8	4.0	100

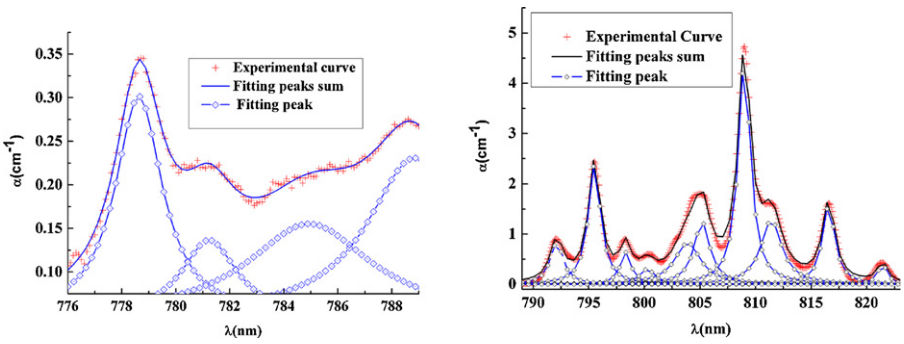

Fig. 4. Peak-fitting of the transitions $|[4I]9/2\rangle \rightarrow |[4F]5/2\rangle$ and $|[4I]9/2\rangle \rightarrow |[2H]9/2\rangle$.

temperature due to weak absorption and thermal peak broadening. The average absorption wavelengths 808.65 nm for $|[4I]9/2\rangle \rightarrow |[4F]5/2\rangle$ and 795.00 nm for $|[4I]9/2\rangle \rightarrow |[2H]9/2\rangle$ were directly used to calculation the multiplet average energy in cm^{-1} with $10^7/\lambda$ (λ in nm), and the obtained energy position of $|[4F]5/2\rangle$ is 12,366.3 cm^{-1}, $|[2H]9/2\rangle$ is 12,578.6 cm^{-1}.

The laser energy systems of Nd:GSAG consist of the pumping level $|[4F]5/2\rangle$, the initial laser-level $|[4F]3/2\rangle$, and the final state $[4I]11/2\rangle$ for emission around 1064 nm or $|[4I]9/2\rangle$ for emission around 942 nm. Then it is necessary to discuss these transitions in some details. Table 4 shows the radiative lifetimes of $|[4F]5/2\rangle$ and $|[4F]3/2\rangle$ are 186 μs and 241 μs, respectively. It seems difficult to achieve population inversion because the lifetime of $|[4F]5/2\rangle$ is relatively long. However, the energy gap between $|[4F]5/2\rangle$ and $|[4F]3/2\rangle$ is only 949 cm^{-1}, the small gap would result in a great phonon transition probability. As a result, it is usually difficult to observe the fluorescence from $|[4F]5/2\rangle$, and the electrons in excited state $|[4F]5/2\rangle$ can relax to $|[4F]3/2\rangle$ quickly to achieve population inversion. The excited state lifetime of $|[4F]3/2\rangle$ we measured is 223 μs, it is less than the theoretical value 241 μs of radiative transition. The nonradiative transition probability P_n can be evaluated by

$$P_n = \frac{1}{\tau^{\exp}} - \frac{1}{\tau^{\mathrm{cal}}} \tag{19}$$

where τ_{cal} and $\tau_{\exp}$ are the theoretical radiative lifetime and experimental excited state lifetime, respectively. The P_n value of $|[4F]3/2\rangle$ calculated is 335 s^{-1}, which is considerable compared with the radiative probability.

The 942 nm and 1064 nm laser of Nd:GSAG compete with each other because they are from the same initial state $|[4F]3/2\rangle$. The fluorescence branch ratios of 942 nm and 1064 nm are 40.6% and 49.1%, respectively. The sum 89.7% is relatively high, which indicates the two transitions are the main laser emission channels of $|[4F]3/2\rangle$. Although 40.6% is smaller than 49.1%, it is still considerable. From the above analysis it shows that the efficiency of 942 nm laser of Nd:GSAG from $|[4F]3/2\rangle \rightarrow |[4I]9/2\rangle$ is high and Nd:GSAG would be a high-efficiency laser medium of 942 nm.

4. Conclusions

Nd:GSAG crystal was grown successfully by Czochralski method, the effective segregation coefficient of Nd^{3+}, refractive indices, and absorption cross sections of Nd^{3+} in GSAG were given by absorption method. The Judd–Ofelt intensity parameters Ω_t ($t = 2, 4, 6$) are fitted as $\Omega_2 = 1.32 \times 10^{-21}$ cm^2, $\Omega_4 = 2.93 \times 10^{-20}$ cm^2 and $\Omega_6 = 3.91 \times 10^{-20}$ cm^2. Meanwhile, the optical transition parameters such as the absorption, emission oscillator strengths, transition probabilities, fluorescence branch ratios, and radiative lifetimes were also derived. The optical transitions of laser operation of Nd^{3+} were analyzed. Higher effective segregation coefficient of Nd^{3+} in GSAG is a major advantage to grow high-doped crystals with high optical quality. Additionally, the large fluorescence ratio of $|[4F]3/2\rangle \rightarrow |[4I]9/2\rangle$ is very favorable for laser operation at 942 nm. These results confirm that Nd:GSAG would be a suitable material for water vapor detection by DIAL.

Acknowledgements

This work is supported by the National Natural Science Foundation of China (Nos. 51002079 and 90922003) and the Natural Science Foundation of the Jiangsu Higher Education Institutions of China (No. 09KJB170003).

References

[1] R. Treichel, C. Czeranowsky, B. Ileri, K. Petermann, G. Huber, Proc. of the 5th ICSO 639, 2004.
[2] F. Kallmeyer, M. Dziedzina, X. Wang, H.J. Eichler, C. Czeranowsky, B. Ileri, K. Petermann, G. Huber, Appl. Phys. B 89 (2007) 305.
[3] S. Wang, X. Wang, F. Kallmeyer, J. Chen, H.J. Eichler, Appl. Phys. B 92 (2008) 43.
[4] H.J. Eichler, F. Kallmeyer, H. Rhee, T. Riesbeck, S. Strohmaier, Proc. SPIE 6346 (2007) 63460Y.
[5] S.G.P. Strohmaier, H.J. Eichler, C. Czeranowsky, B. Ileri, K. Petermann, G. Huber, Opt. Commun. 275 (2007) 170.
[6] L. Zhang, C.Y. Zhang, D.H. Lei, K.N. He, Z.G. Zhang, Z.Y. Wei, H.J. Eichler, Chin. J. Quantum Electron. 24 (2007) 26.
[7] C.W. Xu, Z.Y. Wei, Y.D. Zhang, D.H. Li, Z.G. Zhang, X. Wang, S. Wang, H.J. Eichler, C.Y. Zhang, C.Q. Gao, Opt. Lett. 34 (2009) 2324.
[8] Z.F. Lin, X. Wang, F. Kallmeyer, H.J. Eichler, C.Q. Gao, Opt. Express 18 (2010) 6131.
[9] B.R. Judd, Phys. Rev. 127 (1962) 750.
[10] G.S. Ofelt, J. Chem. Phys. 37 (1962) 511.
[11] D.S. Sumida, M.S. Mangir, D.A. Rockwell, M.D. Shinn, J. Opt. Soc. Am. B: Opt. Phys. 11 (1994) 2066.
[12] S.H. Wemple, W.J. Tabor, J. Appl. Phys. 44 (1973) 1395.
[13] Q.L. Zhang, S.T. Yin, Z.B. Wan, D.L. Sun, S.M. Wan, J. Synth. Crystals 36 (2007) 110.
[14] Q.L. Zhang, S.T. Yin, D.L. Sun, S.M. Wan, Sci. China Ser. G 51 (2008) 481.
[15] A.A. Kaminskii, Crystalline Lasers: Physical Processes and Operating Schemes, CRC Press, Boca Raton, 1996.